Available online at www.sciencedirect.com
ScienceDirect
European Polymer Journal 43 (2007) 599–610
EUROPEAN POLYMER JOURNAL
www.elsevier.com/locate/europolj

Effects of branching characteristics and copolymer composition distribution on non-isothermal crystallization kinetics of metallocene LLDPEs

Mohammad Ashraful Islam [a], Ibnelwaleed A. Hussein [a,*], Muhammad Atiqullah [b]

[a] Department of Chemical Engineering, King Fahd University of Petroleum and Minerals, Dhahran 31261, Saudi Arabia
[b] Center for Refining and Petrochemicals, Research Institute, King Fahd University of Petroleum and Minerals, Dhahran 31261, Saudi Arabia

Received 30 April 2006; received in revised form 21 October 2006; accepted 22 October 2006
Available online 5 December 2006

Abstract

The effects of branch content (BC) and copolymer composition distribution (CCD) on the non-isothermal crystallization kinetics of metallocene m-LLDPEs were studied using modified Avrami analysis, modulated differential scanning calorimetry (MDSC), and Crystaf. Several m-LLDPEs and an m-HDPE – all having comparable M_w and PDI – were experimented. In addition, a ZN-LLDPE was used for comparison purposes. The branch content, unlike the used cooling rates (2–6 °C/min), significantly affected the crystallization behavior. Crystallization peak temperature, T_c^{peak}, decreased linearly with increasing BC. All the m-LLDPEs showed primary and secondary crystallizations. The secondary crystallization showed to be more pronounced at high BC. The primary crystallization Avrami parameter n for m-HDPE ranged between 3.72 and 4.50, indicating spherulitic crystal growth whereas that for the m-LLDPEs, varied from 2.02 to 5.70. The ZN-LLDPE (having broader composition distribution) offered higher values of T_c^{onset} and T_c^{peak} than the m-LLDPEs with similar BC, M_w, and PDI. It, unlike the m-LLDPEs and m-HDPE, fairly agreed with the crystallization kinetic model proposed by Liu et al. The lamella thickness of the m-LLDPEs, L, calculated as per Gibbs–Thomson equation, showed to be in the range 2–16 nm, depending on BC and it decreased approximately following the relationship: L (nm) = $15.0\ e^{(-0.0498BC)}$.

Keywords: Metallocene LLDPE; Branch content; Copolymer composition distribution (CCD); Non-isothermal crystallization; MDSC

1. Introduction

The relationship between microstructure and properties of polymer requires, among other factors, investigation of melting and crystallization behaviors. The microstructure plays an important role in determining the polymer mechanical, optical, rheological, and thermal properties. The study of polymer crystallization kinetics is significant from theoretical and practical points of view [1–9]. A number of studies have been devoted to explore the crystallization behavior of ethylene/α-olefin copolymers [10–15].

* Corresponding author. Tel.: +966 3 860 2235; fax: +966 3 860 4234.
E-mail address: ihussein@kfupm.edu.sa (I.A. Hussein).

0014-3057/$ - see front matter © 2006 Elsevier Ltd. All rights reserved.
doi:10.1016/j.eurpolymj.2006.10.019

The influence of molecular weight (M_w), molecular weight distribution (MWD), the branch type, the branch content (BC), and crystallization conditions on the crystallization behavior of ethylene/α-olefin copolymers have been studied for a long time [16–28]. Most of these studies used Ziegler–Natta linear low density polyethylenes (ZN-LLDPEs). Due to the random comonomer composition and sequence distribution, and intermolecular heterogeneity of ZN-LLDPEs, the effects of the individual factors on the crystallization phenomenon is difficult to separate. For example, for a given short chain BC, the super molecular structure becomes more poorly developed with an increase in the content of high M_w species [16]. On the other hand, with the increase in BC, a lamella first becomes shorter, then segmented, and eventually disintegrates into small crystallites [29]. Also, the previous studies used primarily fractions of conventional heterogeneous ZN-LLDPEs [16,18,21,25,30].

Metallocene LLDPEs (m-LLDPEs) generally have homogeneous composition distribution and narrow MWD. The single-site metallocene catalyst prevents the formation of high and low M_w tails in the resulting copolymers; consequently, m-LLDPEs have more controlled structure. Several studies on the thermal properties and molecular structure of m-LLDPEs have been reported by different authors [26,29,31–41]. Most of these studies focused on the influence of short chain branch distribution [26,31–33,37,40,41] on melting and crystallization kinetics, particularly of a single polymer and its fractions using different fractionation techniques [35,36,38–40]. Bensason et al. [29] classified homogeneous ethylene/1-octene copolymers based on comonomer content and reported the melting phenomena and crystal morphology by relating their results to the tensile and dynamic mechanical properties. However, the influence of BC, branch type, and copolymer composition distribution (CCD) on the crystallization kinetics of m-LLDPEs is yet to be studied. This prompted us to undertake the present study. Our objective is to investigate the effects of BC and CCD on the non-isothermal crystallization kinetics of m-LLDPEs (ethylene/1-butene copolymers) using modulated differential scanning calorimetry (MDSC) [34,42–46] and Crystaf [47]. Note that during processing, the molten polymer crystallizes non-isothermally to form the solid end-products; hence, the study of non-isothermal crystallization kinetics is important [38,48,49].

We have used m-LLDPEs having similar M_w and PDI, and BC in the range of 0–42 branches/1000C. A ZN-LLDPE of the same average BC and M_w has been used to highlight the influence of broader composition distribution on the kinetics of non-isothermal crystallization of LLDPEs. A metallocene high density polyethylene m-HDPE (which is a polyethylene homopolymer having linear backbone) with comparable M_w and PDI has been used as a reference.

2. Experimental

2.1. Materials and sample preparation

Four commercial samples of m-LLDPEs, one ZN-LLDPE and one metallocene high density polyethylene m-HDPE were used in this study. Weight average molecular weights (M_w) of all the LLDPEs (both metallocene and ZN) are close to 100 kg/mol and the PDI of the m-LLDPEs is ≅ 2. Table 1 provides molecular characterization data for all of the polyethylene samples. The density and melt index (MI) values were provided by ExxonMobil. The M_w and BC were determined by gel permeation chromatography (GPC) and ^{13}C NMR, respectively. Details about the GPC and NMR characterizations are available in a previous publication [50]. The experimental polymer samples were named according to their branch type and content. For

Table 1
Molecular characterization of the experimental polymer samples

Experimental samples	Density (g/cm^3)	MI (g/10 min)	M_w (kg/mol)	PDI	BC CH_3/1000C
m-HDPE	N/A	N/A	122	2.34	–
m-EB15	0.910	1.20	108	1.95	14.50
m-EB19	0.900	1.20	110	1.78	18.50
m-EB37	0.888	2.20	87	2.10	36.62
m-EB42	0.880	0.80	126	1.81	42.00
ZN-EB13	0.918	1.0	118	3.07	13.20

Table 2
Operating conditions of Crystaf

Analysis parameters	Values		
	Dissolution	Stabilization[a]	Crystallization
Rate (°C/min)	30.00	30.00	0.20
Temperature (°C)	160	95	30
Time (min)	60	45	0
Total solution volume (ml)			30.00
Sample volume[b] (ml)			1.60
Returned volume (ml)			1.00
Waste volume (ml)			2.50

[a] Slightly above a temperature where crystallization begins.
[b] Volume sampled from the crystallization vessel to obtain each point of the Crystaf curve.

example, a metallocene ethylene/1-butene copolymer with a BC of 18.5 CH_3/1000C is named as m-EB19.

2.2. Measurement of copolymer composition distribution by Crystaf

The copolymer composition distribution of the experimental samples was qualitatively measured using the crystallization fractionation (Crystaf) method. The principle of fractionation is as follows. Crystaf monitors the copolymer solution concentration as the polymer molecules having the same number of side-chain branchings crystallize/precipitate at the same temperature during cooling. Aliquots of the sample solution in trichlorobenzene (TCB) were filtered and analyzed using an infra-red concentration detector. Further details and a description of the Crystaf equipment are available elsewhere [50]. Table 2 summarizes the Crystaf operating conditions.

2.3. Modulated differential scanning calorimetry (MDSC)

Two approaches are presently available for MDSC mode of operation. The first is the reversing and non-reversing heat capacity approach [42]; the second is the complex heat capacity, which can be separated into in-phase and out-of-phase signals using the phase angle [51]. However, the problem associated with complex heat capacity approach is the lack of interpretation of the out-of-phase component that is significantly influenced by the phase angle and thereby by heat transfer effects [52]. Therefore, we have used the first approach.

All the measurements and thermal treatments were performed using a TA Q1000 instrument equipped with a liquid nitrogen cooling system and auto sampler. Nitrogen at a flow rate 50 ml/min was used to purge the instrument to prevent degradation of the samples upon thermal treatments. Polymer samples (7.5–9.8 mg) were sliced and compressed into non-hermetic aluminum pans. To minimize the thermal lag between the sample and the pan, samples with flat surface were used. An empty aluminum pan was used as reference. The previous thermal effects were removed by heating the samples to 140 °C and holding them at this temperature for 5 min. All the samples were cooled to subambient temperatures for complete evaluation of crystallization [25]. The samples were cooled from 140 to 5 °C at a rate of 2 °C/min (with ±0.2 °C modulation), 4 °C/min (with ±0.4 °C modulation) and 6 °C/min with (±0.6 °C modulation) at every 40 s. First, the baseline was calibrated using empty crimped aluminum pans. The calorimeter was calibrated in terms of melting temperature and heat of fusion using a high purity Indium standard (156.6 °C and 28.45 J/g). The absolute crystallinity was calculated using the heat of fusion of a perfect polyethylene crystal, 290 J/g (Ref. [53, p. 347]).

Fig. 1 is a typical MDSC thermogram of sample m-EB15 showing the total (middle curve), reversing (top curve) and non-reversing (bottom curve) heat flow curves. The kinetic data were collected from the non-reversing curve and were processed using

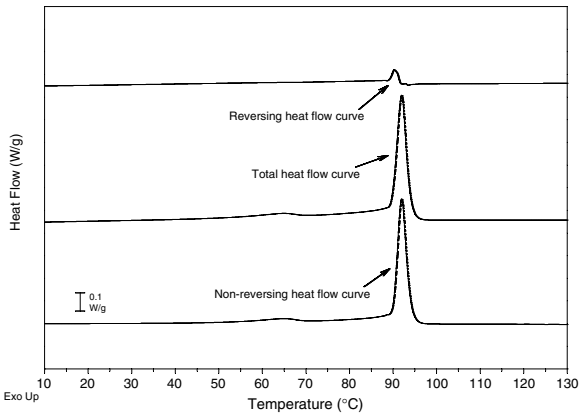

Fig. 1. MDSC thermograms of m-EB15, the three curves from top to the bottom are reversing hear flow, total heat flow and non-reversing heat flow, respectively.

the Universal analysis software provided by TA Instruments, Inc.

3. Results and discussion

3.1. Non-isothermal crystallization and melting behavior

3.1.1. Effects of cooling rates and branch content

The non-isothermal crystallization MDSC traces (non-reversing curves) of the EB LLDPEs (metallocene and ZN) at various cooling rates are shown in Fig. 2a–c. Fig. 2d refers to the thermogram of the reference m-HDPE (cooling rate = 2 °C/min). The LLDPE crystallization exotherms are fairly similar. Independent of the cooling rates, they all show a distinct high temperature peak followed by a minor broad peak to a long tail. This behavior, particularly in the m-LLDPE samples, may be attributed to the non-uniformity in the branch distribution [26,31,33,36,39,41] due to intramolecular compositional heterogeneity [38] combined with primary and secondary crystallizations.The primary crystallization is occurring at higher temperatures corresponding to the appearance of the first major peak. The secondary crystallization is associated with the broadened tail of the thermogram. These two phenomena will be detailed in terms of crystallization kinetics viewpoint later on in Figs. 5–7. A series of physical parameters, obtained from these curves, are listed in Table 3. These parameters include: the onset crystallization temperature (T_c^{onset}), which is the temperature at the crossing point of the tangents of the baseline and the high temperature side of the exotherm; the peak crystallization temperature (T_c^{peak}); overall crystallization

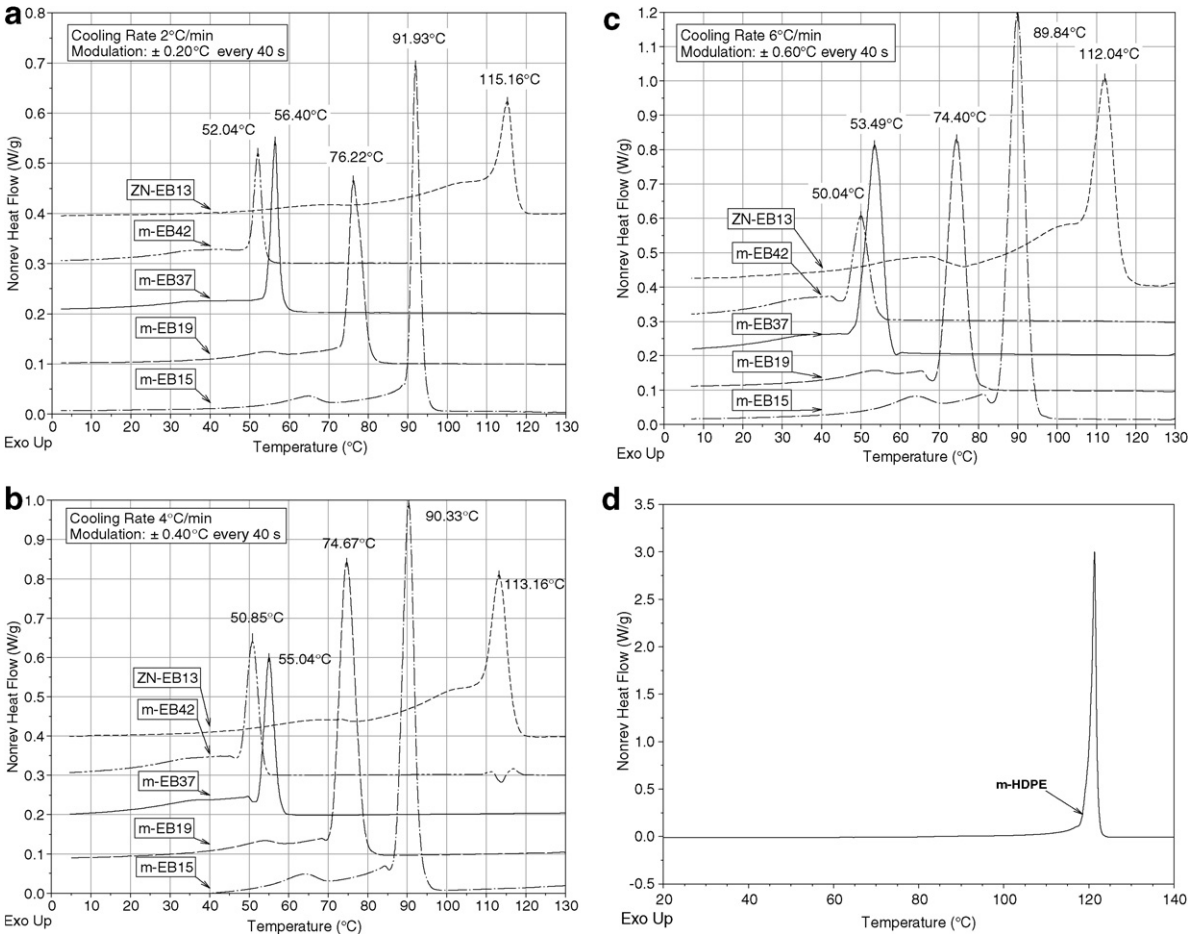

Fig. 2. MDSC non-isothermal crystallization exotherms of EB LLDPEs and m-HDPE. Cooling rates and modulations: (a) 2 °C/min, ±0.2 °C every 40 s; (b) 4 °C/min, ±0.4 °C every 40 s; (c) 6 °C/min, ±0.6 °C every 40 s; (d) m-HDPE, 2 °C/min, ±0.2 °C every 40 s, respectively.

Table 3
Crystallization parameters and thermodynamic properties for the experimental ethylene/1-butene copolymers

R (°C/min)	Experimental samples	T_c^{onset} (°C)	T_c^{peak} (°C)	$t_{1/2}$ (min)	ΔH_c (J/g)	X_c (%)
2	m-HDPE	122.05	121.34	0.91	195.9	67.55
	m-EB15	94.04	91.93	1.82	86.51	29.83
	m-EB19	80.22	76.22	2.35	65.25	22.5
	m-EB37	58.06	56.40	2.44	43.78	15.10
	m-EB42	53.88	52.04	4.98	36.19	12.48
	ZN-EB13	117.77	115.16	7.32	89.83	30.98
4	m-HDPE	121.80	120.60	1.03	123.30	42.50
	m-EB15	93.02	90.33	1.54	80.92	27.90
	m-EB19	78.92	74.67	1.94	71.91	24.80
	m-EB37	57.57	55.04	2.44	34.66	11.95
	m-EB42	53.67	50.85	2.29	34.32	11.83
	ZN-EB13	116.95	113.16	3.82	88.65	30.57
6	m-HDPE	121.77	119.47	1.01	173.0	59.67
	m-EB15	93.68	89.84	1.82	81.29	28.03
	m-EB19	78.37	74.40	1.92	53.94	18.60
	m-EB37	57.27	53.49	1.61	42.54	14.67
	m-EB42	53.89	50.04	1.8	27.65	9.54
	ZN-EB13	116.40	112.04	2.28	87.79	30.27

half-time ($t_{1/2}$); the enthalpy of crystallization (ΔH_c), and absolute crystallinity (X_c). The $t_{1/2}$ was calculated directly from the MDSC non-reversing exotherms where the absolute crystallinity is 50%.

The cooling rate (2–6 °C/min) hardly influenced T_c^{onset} and T_c^{peak} of all the samples (Table 3). Fig. 3 shows the change of T_c^{peak} with BC for the m-LLDPEs. A linear relationship (T_{Peak} (°C) = − 1.6BC + 115) between T_c^{peak} and BC was observed at all cooling rates. This relationship is similar to that proposed by Hosoda [54] (T_{melt} (°C) = −1.6BC + 136) and confirmed by other researchers [55,56] for ethylene/1-butene copolymers produced by Ziegler–Natta catalysts. ZN-EB13, for all the experimental cooling rates, showed higher crystallization parameters (T_c^{onset}, T_c^{peak}, $t_{1/2}$, and ΔH_c) than the m-EB15 having similar M_w and BC (Table 3). However, X_c turned out to be fairly comparable. This is attributed to the difference in composition distribution between m-EB15 and ZN-EB13, and the presence of linear fractions in ZN-EB13 [21,26,41]. Note that $\sigma_{crystaf}$, a measure of copolymer compositional heterogeneity, is 3.6, 3.9, and 15.1 for m-EB15, m-EB19, and ZN-EB13, respectively. The crystallization enthalpy (ΔH_c) as well as absolute crystallinity (X_c) decreased with increasing BC for the m-LLDPEs (Table 3).

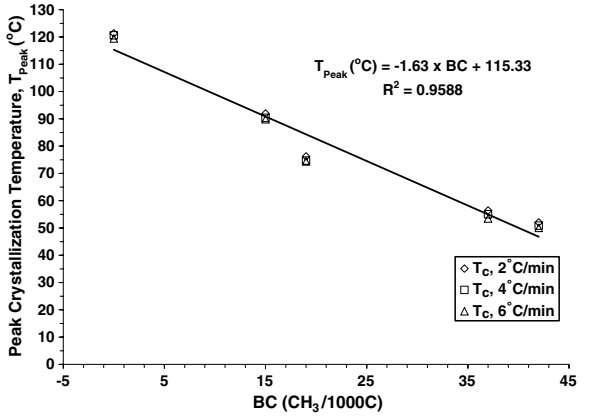

Fig. 3. Variation of peak crystallization temperature (T_c^{peak}) as function of BC (CH_3/1000C) at various cooling rates for the m-LLDPEs.

In addition, T_c^{onset} and T_c^{peak} of all the m-LLDPEs were lower than those of the m-HDPE (122 °C; 121 °C; cooling rate 2 °C/min, Fig. 2d). On the other hand, ZN-LLDPE (BC = 13 CH_3/1000C) displayed strong peaks at 115, 113, and 112 °C corresponding to 2, 4, and 6 °C/min, respectively (Fig. 2a–c). These peaks represent the linear backbone fractions in ZN-LLDPE and are usually observed at ~90 °C in temperature rising elution fractionation (TREF) measurements [26]. In our work, we found the corresponding values determined by Crystaf to be in the range 80–90 °C (Fig. 4). The absence of the 112–115 °C peaks in m-EB15, which has a similar BC and M_w as ZN-EB13, suggests the absence of crystal populations representing linear backbone fractions. This is consistent with the fact that m-LLDPE molecules were made by a single-site metallocene

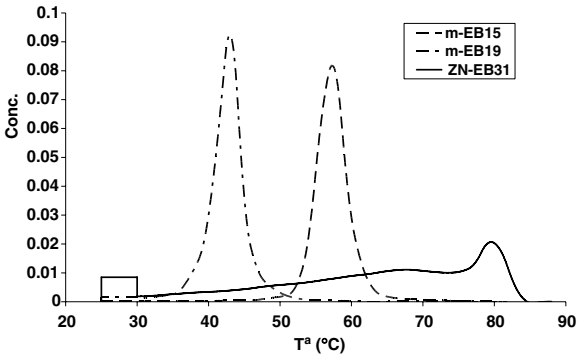

Fig. 4. Crystaf analysis of the selected experimental samples.

catalyst, which produced uniform branches. Also, the T_c^{onset} and T_c^{peak} of the m-LLDPEs shifted to lower values ($\leqslant$94 °C) depending on BC. We observed another broad and weak tail and the size of the observed tail increased with increasing BC. This tail did not appear in the thermogram of the m-HDPE (Fig. 2d). Analysis of these samples by Crystaf (Fig. 4) shows uniform composition distribution, hence the presence of only one type of crystal structure in m-LLDPEs. On the other hand, in Fig. 2 ZN-EB13 showed two crystal populations representing the linear and the branched molecules. The highly branched m-LLDPEs (m-EB37 and m-EB42; ~40 CH_3/1000C) did not show any peak in Crystaf; just a straight line coinciding with the x-axis. This suggests that the chain folding of m-LLDPEs in solution requires a methylene sequence of more than 25C (<40 branches/1000C). However, in the melt the polymer will crystallize as shown in the DSC plots.

3.2. Non-isothermal crystallization kinetics

Several models have been developed to describe the non-isothermal crystallization kinetics of polymers: (1) the modified Avrami analysis [3,57–59]; (2) the Ozawa analysis [2]; (3) Ziabicki analysis [60,61]; and others [62–65]. In this study, the modified Avrami analysis proposed by Jeziorny [3] and a kinetic model suggested by Liu et al. [60] were used to describe the non-isothermal crystallization kinetics of m-LLDPEs. Due to the variation in the range of crystallization temperature, Ozawa model [2] was not suitable for this study.

The Avrami equation, developed based on the assumption of constant crystallization temperature, is defined as follows [66–68]:

$$1 - X_t = \exp(-k_t t^n) \tag{1}$$

where n is the Avrami crystallization exponent dependent on the nucleation mechanism and growth dimension, t is the time taken during the crystallization process, k_t is the growth rate constant, which depends on nucleation and crystal growth, and X_t is the relative crystallinity [69]. The relative crystallinity, X_t is defined as follows:

$$X_t = \frac{\int_{t_o}^{t} (\mathrm{d}H_c/\mathrm{d}t)\mathrm{d}t}{\int_{t_o}^{t_\infty} (\mathrm{d}H_c/\mathrm{d}t)\mathrm{d}t} \tag{2}$$

where $\mathrm{d}H_c/\mathrm{d}t$ is the rate of heat evolution, and t_o and t_∞ are the onset and completion times of the crystallization process, respectively.

Jeziorny [3] modified Eq. (1) to describe non-isothermal crystallization. At a chosen cooling rate, the relative crystallinity is a function of the crystallization temperature (T). That is, Eq. (2) can be formulated as

$$X_T = \frac{\int_{T_o}^{T_c} (\mathrm{d}H_c/\mathrm{d}T)\mathrm{d}T}{\int_{T_o}^{T_\infty} (\mathrm{d}H_c/\mathrm{d}T)\mathrm{d}T} \tag{3}$$

where T_o denotes the onset crystallization temperature, and T_c and T_∞ represent the crystallization temperature at time t and after the completion of the crystallization process, respectively. Crystallization time, t, can be converted from crystallization temperature, T_c, using the following equation [3,61] (that is strictly valid when the sample experiences the same thermal history).

$$t = \frac{T_o - T}{R} \tag{4}$$

where R is the cooling rate (°C/min). The double-logarithmic form of Eq. (1) yields

$$\ln[-\ln[1 - X_t]] = \ln k_t + n \ln t \tag{5}$$

Thus, the Avrami exponent n and the crystallization rate constant k_t can be obtained from the slope and the intercept of the plot of $\ln[-\ln(1 - X_c)]$ vs $\ln t$, respectively, for each cooling rate. The physical meaning of k_t and n cannot be related to the non-isothermal case in a simple way; they provide further insight into the kinetics of non-isothermal crystallization. The rate of non-isothermal crystallization depends on the cooling rate. Therefore, k_t of Eqs. (1) and (5) can be corrected to obtain the corresponding rate constant at a unit cooling rate, k_R [3]:

$$\ln k_R = \ln k_t / R \tag{6}$$

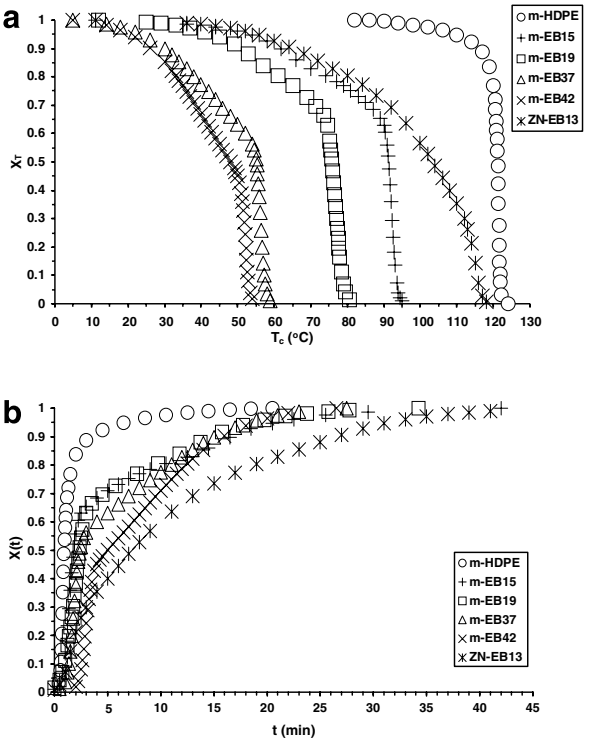

Fig. 5. Relative crystallinity as a function of (a) crystallization temperature, T_c and (b) modified crystallization time, t for the experimental samples. Cooling rate and modulation: 2 °C/min, ±0.2 °C every 40 s, respectively.

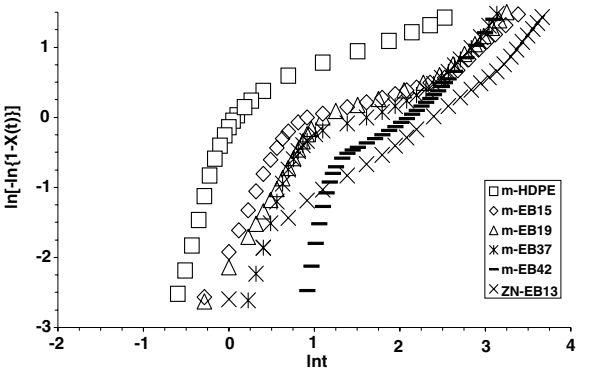

Fig. 6. Primary crystallization Avrami plots for the experimental samples. Cooling rate and modulation: 2 °C/min, ±0.2 °C every 40 s, respectively.

The crystallization exotherm data obtained at a cooling rate 2 °C/min is shown in Fig. 5(a). The relative crystallinity (X_t) as a function of temperature was calculated using Eq. (3). Once X_t is obtained, it can be converted into X_t by transforming the temperature axis to the modified time analogue using Eq. (4). X_t versus the modified non-isothermal crystallization time is plotted in Fig. 5(b). Each m-LLDPE, except the m-HDPE, shows a strong and sharp exothermic peak, followed by a weak and broad long tail at lower temperatures. As a result of the broad composition distribution (Fig. 4), ZN-EB13 showed a gradual increase in crystallinity with time, while m-EB15 (having similar BC) showed a sharper crystallization peak. Also, crystallization started earlier in ZN-EB13 than in m-EB15. In other words, the compositional homogeneity in m-EB15 increased its capability of crystallization over that of ZN-EB13 having significantly inhomogeneous composition (Fig. 4).

Initially, an attempt was made to fit the whole data of EB m-LLDPEs and m-HDPE using the Avrami analysis as shown in Fig. 6. The m-LLDPEs showed an initial linear portion, then a plateau followed by another linear part. However, the Avrami plot for ZN-LLDPE was mostly linear over the whole range. This difference between ZN-LLDPE and m-LLDPEs is due to the heterogeneity in composition distribution in ZN-LLDPE (Fig. 4). In ZN-LLDPE, linear molecules dominate the crystallization process. Similar deviations in Avrami plots were reported by several authors in similar crystallization studies. For example, see the results of Jiao et al. Fig. 6a of Ref. [28]; Janimak and Stevens Fig. 5 of Ref. [34] for m-LLDPE and Liu et al. Fig. 7 of Ref. [62] for copolyterephthalamide. Janimak and Stevens [34] used a single line to fit the whole set of data applying the least square method. In this study, it was found that the initial linear portion of those curves mentioned in Fig. 6 represents, in most cases, more than 70% crystallinity. Fig. 7a–c represent the Avrami plots of the major crystallization portion of EB m-LLDPEs and m-HDPE at 2, 4 and 6 °C/min, respectively.

The values of n, k_t, k_R, and coefficient of determination (R^2) are listed in Table 4. Fig. 8 shows uncorrelated relationship between the Avrami exponents and BC at the three different cooling rates. The value of n for m-HDPE varied between 3.72 and 4.50. This matches with the published literature report, that is, m-HDPE exhibits spherulitic growth having n values in the range of 3–4 [70]. On the other hand, for the m-LLDPEs, n varied from 2.02 to 5.70. This variational range differs from what has been reported mostly for ZN-LLDPEs, $1 \leqslant n \leqslant 2$ [18]. Our ZN-LLDPE n values (see Table 4) agree with what the literature reports. The present study shows that m-LLDPEs, unlike ZN-LLDPEs, can have a wider n-range. The value of n is usually an integer varying

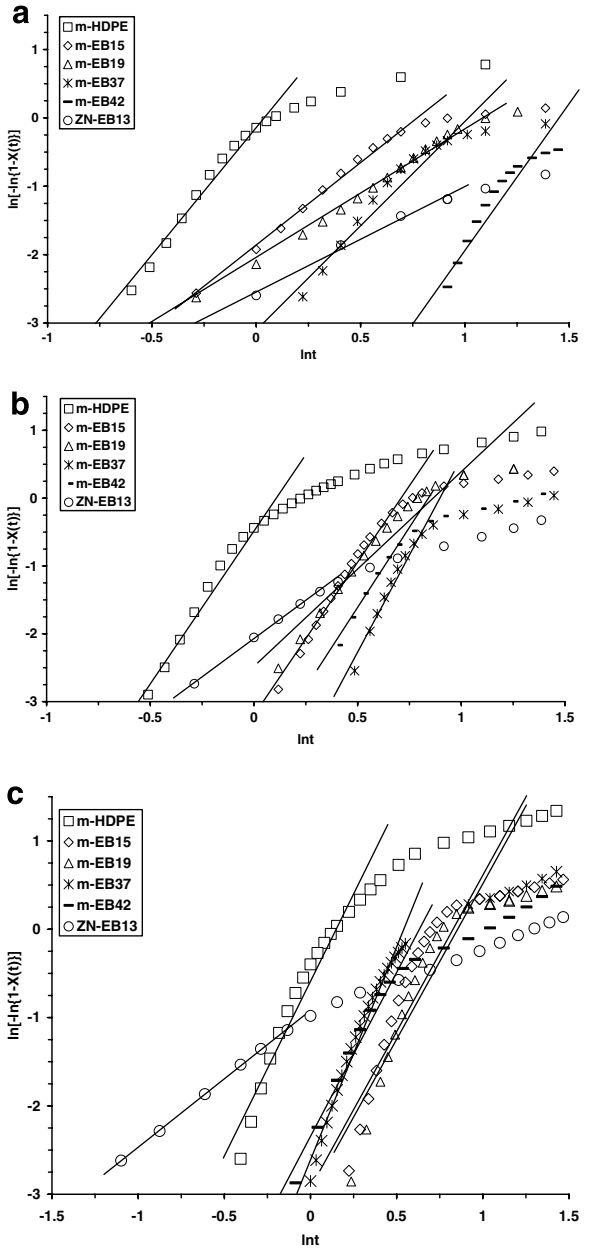

Fig. 7. Avrami plots for m-EB LLDPEs, ZN-EB13, and m-HDPE for the primary crystallization range. Cooling rates and modulations: (a) 2 °C/min, ±0.2°C every 40 s; (b) 4 °C/min, ±0.4 °C every 40 s; (c) 6 °C/min, ±0.6 °C every 40 s, respectively.

between 1 and 4, and is dependent on crystallization mechanisms. It is a fraction for secondary crystallization [71]. Wunderlich [69] suggested that the mechanism of secondary crystallization is either a crystal perfection process or a crystal thickness growth. But this was opposed by Strobl et al. [17]. They suggested that BC hinders longitudinal chain diffusion through the crystals, thus suppresses crystal thickness growth. So, a very slow further lateral extension of lamella was suggested to occur during secondary crystallization. Strobl et al. [17] observations were confirmed by SAXS experiments.

Our DSC thermograms of the m-LLDPE samples showed a long tail (secondary crystallization as per Wunderlich [69]). The dependency of the crystallization rate constant, k_R, on BC and cooling rates is shown in Fig. 9. Corresponding to the cooling rates of 2 and 4 °C/min, k_R fairly exponentially decreased as a function of BC. However, for the cooling rate of 6 °C/min, k_R decreased up to BC = 15; then it remained fairly constant. These findings may be attributed to decreasing chain-folding capability caused by the increasing BC. For a given BC, k_R increased with the increase in cooling rate. This so happened due to faster extraction of thermal energy.

Further, a kinetic model proposed by Liu et al. [62] was tried. However, this kinetic model did not provide a good fit for the m-HDPE and the m-LLDPEs. Only ZN-EB13 showed a fair fit (see Fig. 10). Therefore, a ZN-LLDPE, due to heterogeneity in copolymer composition, can provide a fair agreement with the kinetic model proposed by Liu et al.

3.3. Correlation of crystal thickness to branch content

The DSC data were also analyzed to correlate crystal thickness to branch content. The crystal thickness L can be related to the melting temperature (T_m) by rearranging the Gibbs–Thomson equation as follows:

$$\frac{L}{\sigma_e} = \frac{2}{(\Delta H_m^0 \cdot \rho_c)} \left[1 - \frac{T_m}{T_m^0}\right]^{-1} \tag{7}$$

where T_m^0, is the melting temperature of a polyethylene crystal of infinite thickness (414.6 K) [Ref. [53], p. 359]; ΔH_m^0, the heat of melting of the perfect crystal (290 J/g) [Ref. [53], p. 347]; and σ_e, the surface energy which is of the order of 100 erg/cm^2 for regular folding [72]. Considering the equivalence of equilibrium melting and crystallization, Eq. (7) was written as

$$\frac{L}{\sigma_e} = \frac{2}{(\Delta H_c^0 \cdot \rho_c)} \left[1 - \frac{T_c}{T_c^0}\right]^{-1} \tag{8}$$

The derivative of the cumulative crystallinity with respect to T_c yields an incremental crystal fraction, ϕ', that can reveal more clearly the crystallization behavior of the experimental polymers [73]. When

Table 4
Primary crystallization Avrami parameters for the experimental ethylene/1-butene copolymers

Cooling rate and modulation	Experimental samples	Major primary crystallization parameters			
		n	k_t	k_R	R^2
2 °C/min, ±0.2 °C every 40 s	m-HDPE	3.72	0.868	0.932	0.988
	m-EB15	2.55	0.153	0.392	0.998
	m-EB19	2.02	0.119	0.345	0.998
	m-EB37	3.05	0.045	0.212	0.954
	m-EB42	4.30	0.002	0.044	0.908
	ZN-EB13	1.54	0.078	0.280	0.997
4 °C/min, ±0.4 °C every 40 s	m-HDPE	4.51	0.616	0.886	0.983
	m-EB15	4.51	0.041	0.449	0.982
	m-EB19	3.05	0.073	0.520	0.930
	m-EB37	5.72	0.006	0.277	0.969
	m-EB42	4.72	0.019	0.371	0.980
	ZN-EB13	2.26	0.126	0.596	0.999
6 °C/min, ±0.6 °C every 40 s	m-HDPE	3.96	0.555	0.906	0.950
	m-EB15	3.54	0.054	0.614	0.830
	m-EB19	3.52	0.049	0.606	0.857
	m-EB37	4.82	0.073	0.647	0.980
	m-EB42	3.71	0.096	0.677	0.971
	ZN-EB13	1.54	0.399	0.858	1.00

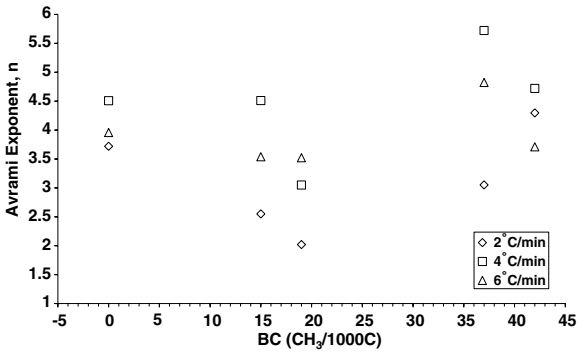

Fig. 8. Effect of BC on the Avrami exponents at different cooling rates.

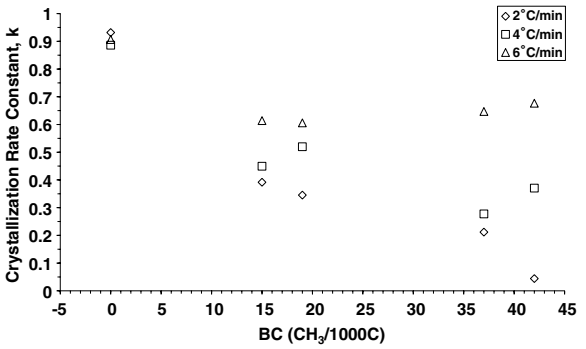

Fig. 9. Effect of BC on the crystallization rate constant at various cooling rates.

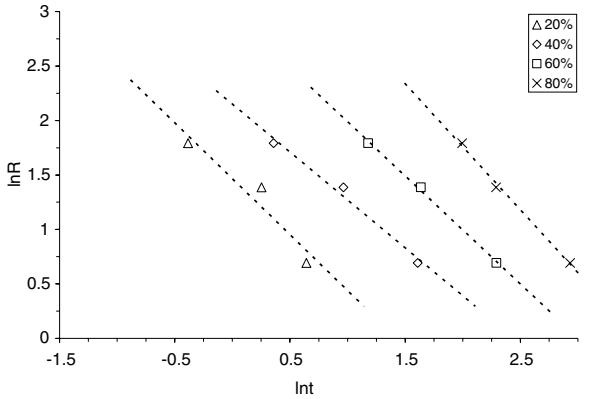

Fig. 10. Plots of $\ln R$ vs $\ln t$ at each given relative crystallization, $X(t)$ for ZN-EB13.

ϕ' is plotted as a function of $\frac{L}{\sigma_e}$ (Fig. 11), the m-HDPE shows a single peak with sharp crystallization peak at low cooling rate. As BC increases, a second smaller peak appears as a tail as shown in the previous data. Figs. 11 and 12 inform the same on the relation between BC and diffusion limitations in crystallization from the melt. However, the correlation is more obvious when the derivative of the cumulative crystallinity was used (Fig. 11). In the case of ZN-EB13, three peaks were obtained, which suggests multiple crystal populations associated with linear, branched and co-crystals [41] as illustrated by the broad copolymer composition

distribution (see Fig. 4). ZN-LLDPE possesses both inter- and intra-molecular heterogeneities, while m-LLDPEs are of mainly uniform composition distribution. A comparison of the results of ϕ' (Fig. 11e and f) for high BC m-LLDPE and ZN-LLDPE suggests that the cooling rate more strongly affects the crystallization of m-LLDPE than that of ZN-LLDPE of similar M_w and average BC.

The $\frac{L}{\sigma_e}$ ratio is a measure of the combined effects of the comonomer content on crystal thickness and surface order. When there are two peaks, it suggests that there are two crystal populations [73]. If the above value of σ_e was used, the maximum crystal thickness L could be calculated and correlated to BC for m-LLDPEs. Results are given in Fig. 12. Values of L are in the range 2-16 nm depending on BC. The decrease of L with BC follows approximately the relation: $L\ (\text{nm}) = 15.0\, e^{(-0.0498\times BC)}$. Now we shall evaluate this relation considering the limiting case of a linear polyethylene for which results are available in the literature. Wunderlich (see Ref. [53, p. 372]) showed that for linear PE

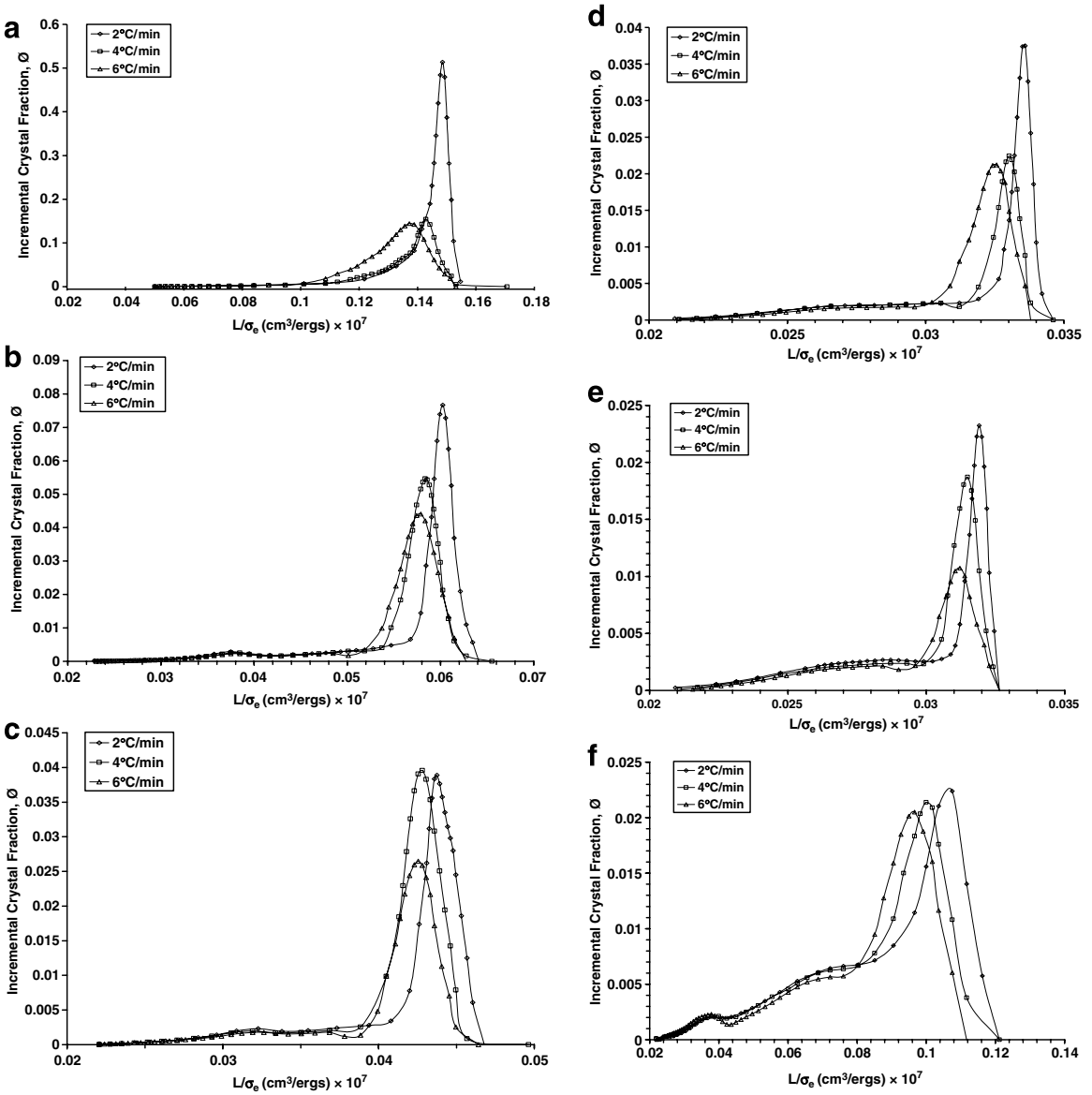

Fig. 11. Incremental crystal fraction of (a) m-HDPE, (b) m-EB15, (c) m-EB19, (d) m-EB37, (e) m-EB42, (f) ZN-EB13 as function of $\frac{L}{\sigma_e}$ at various cooling rates.

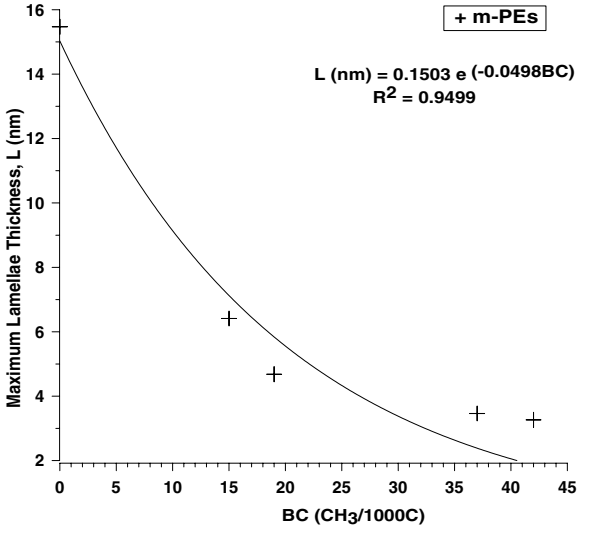

Fig. 12. Maximum lamellae thickness calculated as a function of BC using Eq. (9).

the melting temperature as a function of lamella thickness is given by

$$T_m = 414.2\left(1 - \frac{0.627}{L}\right) \; L \text{ in nm, error} \pm 0.8 \text{ K} \tag{9}$$

If we take the linear m-HDPE as an example, the lamellar thickness is ~15 nm which, according to Eq. (9), shows a melting temperature of 123.7 °C. From Table 3, the onset crystallization temperature of m-HDPE is 122.05 °C. This result is almost in agreement with the prediction of Eq. (9).

4. Conclusions

Based on the previous results and discussion, the following can be concluded:

1. The non-isothermal crystallization of m-LLDPEs occurred through primary and secondary crystallization processes. A large fraction of crystallinity was developed by the slow secondary crystallization process.
2. The peak crystallization temperature, T_c^{peak}, and the crystallization onset temperature, T_c^{onset}, were strongly influenced by BC. It moved to a lower temperature region as BC increased. The cooling rate (2–6 °C/min) hardly influenced T_c^{peak}. However, T_c^{onset} mildly increased when the cooling rate was decreased. However, the copolymer composition distribution (CCD), unlike the cooling rate, significantly affected T_c^{peak} and T_c^{onset}. The ZN-EB13, for all the experimental cooling rates, showed higher crystallization parameters (T_c^{onset}, T_c^{peak}, $t_{1/2}$, and ΔH_c) than the m-EB15 having similar M_w and BC. However, X_c turned out to be fairly comparable.
3. The absolute crystallinity, X_c, was influenced by BC and CCD. Increase in BC lowered X_c. Also, ZN-LLDPE with broader CCD showed higher absolute crystallinity than m-LLDPEs having similar BC and M_w.
4. The value of n, under the experimental cooling rates, for m-HDPE ranged between 3.72 and 4.50, indicating spherulitic crystal growth. On the other hand, for the m-LLDPEs, n varied from 2.02 to 5.70. This variational range differs from what has been reported mostly for ZN-LLDPEs, $1 \leqslant n \leqslant 2$. Therefore, m-LLDPEs, unlike ZN-LLDPEs, can have a wider n-range. This finding will stimulate future research on LLDPE crystallization mechanism.
5. The crystallization kinetic model proposed by Liu et al. [62] did not apply to the m-LLDPEs (having narrow copolymer composition distribution) and m-HDPE. However, it fairly worked for ZN-LLDPE having pronounced heterogeneity in copolymer composition distribution.
6. The lamella thickness of the LLDPEs, L, calculated as per Gibbs–Thomson equation, showed to be in the range 2–16 nm, depending on BC and it decreased approximately following the relationship: L (nm) = 15.0 $e^{(-0.0498\times BC)}$.

Acknowledgements

The authors are grateful to King Abdul Aziz City for Science and Technology (KASCT) for providing financial support for this research under research Grant # AT-22-16. They also acknowledge the support of King Fahd University of Petroleum and Minerals (KFUPM), Dhahran 31261, Saudi Arabia. Acknowledgement is also extended to ExxonMobil for providing the polymer samples and to Polychar at Spain for the Crystaf analysis.

References

[1] Evans UR. Trans Faraday Soc 1945;41:365.
[2] Ozawa T. Polymer 1971;12:150.
[3] Jeziorny A. Polymer 1978;19:1142.
[4] Hay JN, Mills PJ. Polymer 1982;23:1380.
[5] McHugh AJ, Burghardt WR, Holland DA. Polymer 1986;27:1585.

[6] Parasnis NC, Ramani K. J Therm Anal Calorim 1999;55:709.
[7] Jayakannan M, Ramakrishnan S. J Appl Polym Sci 1999;74:59.
[8] Sajkiewicz P, Carpaneto L, Wasiak A. Polymer 2001;42:5365.
[9] Qui Z, Ikehara T, Nishi T. Polymer 2003;44:5429.
[10] Kao YH, Phillips PJ. Polymer 1986;27:1669.
[11] Phillips PJ, Kao YH. Polymer 1986;27:1679.
[12] Nordmeier E, Lanver U, Lechner MD. Macromolecules 1990;23:1072.
[13] Sutton SJ, Vaughan AS, Bassett DC. Polymer 1996;37(25):5735.
[14] Wagner J, Abu-Iqyas S, Monar K, Phillips PJ. Polymer 1999;40:4717.
[15] Wagner J, Phillips PJ. Polymer 2001;42:8999.
[16] Mandelkern L, Maxfield J. J Polym Sci: Polym Phys Ed 1979;17:1913.
[17] Strobl GR, Engelke T, Maderek E, Urban G. Polymer 1983;24:1585.
[18] Maderek E, Strobl GR. Colloid Polym Sci 1983;261:471.
[19] Alamo R, Domszy R, Mandelkern L. J Phys Chem 1984;88:6587.
[20] Mandelkern L. Polym J 1985;17:337.
[21] Usami T, Gotoh Y, Takayama S. Macromolecules 1986;19:2722.
[22] Alamo RG, Mandelkern L. Macromolecules 1989;22:1273.
[23] Fatou JG, Marco C, Mandelkern L. Polymer 1990;31:1685.
[24] Alamo RG, Viers BD, Mandelkern L. Macromolecules 1993;26:5740.
[25] Shanks RA, Amarasinghe G. J Therm Anal Calorim 2000;59:471.
[26] Zhang M, Lynch DT, Wanke SE. Polymer 2001;42:3067.
[27] Rabiej S, Goderis B, Janicki J, Mathot VBF, Koch MHJ, Groeninckx G, et al. Polymer 2004;45:8761.
[28] Jiao C, Wang Z, Liang X, Hu Y. Polym Test 2005;24:71.
[29] Bensason S, Minick J, Moet A, Chum S, Hiltner A, Baer E. J Polym Sci: Polym Phys Ed 1996;34:1301.
[30] Voigt-Martin IG, Alamo R, Mandelkern L. J Polym Sci: Polym Phys Ed 1986;24:1283.
[31] Keating MY, Lee IH. J Macromol Sci Phys 1999;B38:379.
[32] Starck P, Lehmus P, Seppala V. Polym Engng Sci 1999;39:1444.
[33] Xu J, Xu X, Feng L. Eur Polym J 1999;36:685.
[34] Janimak JJ, Stevens GC. Thermochim Acta 1999;332:125.
[35] Razavi-Nouri M, Hay JN. Polymer 2001;42:8621.
[36] Fu Q, Chiu F-C, He T, Liu J, Hsieh ET. Macromol Chem Phys 2001;202:927.
[37] Wang C, Chu MC, Lin TL, Lai SM, Shih HH. Polymer 2001;42:1733.
[38] Chiu F, Fu Q, Peng Y, Shih H. J Polym Sci Part B: Polym Phys 2002;40:325.
[39] Starck P, Löfgren B. Eur Polym J 2002;38:97.
[40] Teng H, Shi Y, Jin X. J Polym Sci Part B: Polym Phys 2002;40:2107.
[41] Hussein IA. Polym Int 2004;53(9):1327.
[42] Gill PS, Sauerbrunn SR, Reading M. J Therm Anal 1993;40:931.
[43] Reading M, Elliott D, Hill VL. J Therm Anal 1993;40:949.
[44] Okazaki I, Wunderlich B. Macromol Rapid Commun 1997;18:313.
[45] Yuan ZH, Song R, Shen DY. Polym Int 2000;49:1377.
[46] Qui ZB, Ikehara T, Nishi T. Polymer 2003;44:3095.
[47] Monrabal B. J Appl Polym Sci 1994;52:491.
[48] Pick LT, Harkin-Jones E, Oliveira MJ, Cramez MC. J Appl Polym Sci 2006;101:1963.
[49] Run M, Gao J, Li Z. Thermochim Acta 2005;429:171.
[50] Hameed T, Hussein IA. Polymer 2002;43:6911.
[51] Schawe JEK. Thermochim Acta 1995;260:1.
[52] Righetti MC. Thermochim Acta 1999;330:131.
[53] Wunderlich B. 2nd ed. In: Turi EA, editor. Thermal characterization of polymeric materials, vol. 1. New York: Academic Press; 1997.
[54] Hosoda D. Polym J 1988;20:383.
[55] Adisson E, Ribeiro M, Deffieux A, Fontanille M. Polymer 1992;33:4337.
[56] Starck P. Polym Int 1996;40:111.
[57] Tobin MC. J Polym Sci: Polym Phys Ed 1974;12:399.
[58] Rychly J, Janigova I. Thermochim Acta 1993;215:211.
[59] Herrero CH, Acosta JL. Polym J 1994;26:786.
[60] Ziabbicki A. Colloid Polym Sci 1974;6:252.
[61] Ziabbicki A. Appl Polym Symp 1967;6:1.
[62] Liu TX, Mo ZS, Wang SE, Zhang HF. Polym Eng Sci 1997;37:568.
[63] Caze C, Devaux E, Crespy A, Cavrot JP. Polymer 1997;38:497.
[64] Nakamura K, Katayama K, Amano T. J Appl Polym Sci 1973;17:1031.
[65] Chan TW, Isayev AI. Polym Engng Sci 1994;34:461.
[66] Avrami M. J Chem Phys 1939;7:1103.
[67] Avrami M. J Chem Phys 1940;8:212.
[68] Avrami M. J Chem Phys 1941;9:177.
[69] Wunderlich B. Macromol Phys, vol. 2. New York: Academic Press; 1976. p. 147.
[70] Buchdahl R, Miller RL, Newman S. J Polym Sci 1959;36:215.
[71] Chen K, Tang X, Shen J, Zhou Y, Zhang B. Macromol Mat Engng 2004;289:539.
[72] Frank FC, Tossi M. Proc R Soc Lond A 1961;263:323.
[73] Minick J, Moet A, Hiltner A, Baer E, Chum SP. J Appl Polym Sci 1995;58:1371.